Third Body Influence on Thermal Friction Contact Problems: Application to Braking

Didier Majcherczak
e-mail: Didier.Majcherczak@polytech-lille.fr

Philippe Dufrénoy
e-mail: Philippe.dufrenoy@polytech-lille.fr

Moussa Naït-Abdelaziz
e-mail: Moussa.nait-abdelaziz@polytech-lille.fr

Laboratoire de Mécanique
de Lille—CNRS UMR 8107,
Ecole Polytechnique Universitaire de Lille,
59655 Villeneuve d'ascq, France

The aim of this study is to evaluate the temperature and the heat distribution into the two components of a disc brake system by combining macroscopic and microscopic effects. The major difficulty of the thermal problem is to determine how the heat is generated and how it is distributed in the two components in contact during transient state. Contrary to classical approaches assuming equal temperature at the contact surfaces, a contact interface is introduced in the model as a thin layer of third body with uniform volumic heat generation. This micro-macro model gives original indications on the temperatures near the contact surfaces, on the thermal gradients between the two components and on the heat partition between the two bodies during the braking time. Comparison with classical thermal models is discussed. [DOI: 10.1115/1.1757490]

Keywords: third body, thermal contact, heat partition, braking

1 Introduction

In frictional problems, two major difficulties remain in the thermal modeling of the components in sliding contact: (1) the coupling phenomena between tribological, mechanical and thermal behavior with materials degradations [1]; and (2) the multi-scale aspect, from the local heat generation to the volumic thermal dissipation [2].

On a tribological point of view, size of real contact surface is highly reduced compared to apparent contact area. On this real contact surface, a relative speed accommodation takes place by [3,4] first body surfaces degradation (disc and pads) and third body shearing.

Damages may be micro-cracks and superficial tribological transformations (STT) which affect the first bodies near the contact surfaces (in a thickness of about fifty micrometers depth).

In disc brakes, the thermal problem is of an eminent importance. The heat generated during braking involves temperature rise in the brake components that affects brake performances, and modifies friction properties and wear process.

Although thermal and tribological effects are coupled, the thermal problem is generally separately solved by assuming thermal continuity at the interface.

In this work, the goal we purchase is to introduce in the thermal problem, an interface layer modelled from tribological considerations. The aim is to better understand the mechanisms of heat generation and to give original indications on the temperatures near the contact surface. The mechanical aspects are deliberately ignored here.

In the first part, classical analytical solutions are reminded. In a second part, numerical models with assumptions of thermal interface continuity are described and compared to analytical solutions. In the last part, the introduction of an interface layer in a finite element model is presented and results are discussed.

2 Macroscopic Models of Heat Dissipation in Discs Brake

The thermal problem needs to deal with the following aspects [2]: the conversion of the kinetic energy into dissipated heat induced by friction; and the heat partition between the disc and the pads (thermal contact description). The deceleration is assumed to be constant. The major part of the energy is kinematic and the mechanical energy is assumed to be completely converted into heat. One can write

$$E_c + Q = 0 \quad \text{with} \quad E_c \approx \frac{1}{2} m V_0^2$$

From this basic data of the global energy to dissipate, partition of the heat flux between disc and pads cannot be easily estimated. Some authors propose to evaluate this partition according to the thermal characteristics and assuming equal surface temperature (perfect contact). Nevertheless, as the problem is highly transient and open on thermodynamic point of view, thermal equilibrium cannot be obtained at each moment. Another consideration is that surface contact is imperfect, with third body interface layers (imperfect contact) [3].

Solving the thermal problem requires to formulate assumptions which essentially concerns the thermal contact conditions: perfect and imperfect contacts

2.1 Thermal Contact Description

2.1.1 Perfect Contact. The main problem is to determine the heat flux quantity dissipated by the two solids in contact. This point is solved by Archard [5] who has determined the fraction of flux into the solids assuming that the mean temperatures of the two surfaces in contact are equal. The heat flux dissipated by each component depends on the heat flux partition coefficient, p as follows (Eq. 1)

$$\phi_1 = p \cdot \phi \quad \text{et} \quad \phi_2 = (1-p)\phi \tag{1}$$

with ϕ the total heat flux generated by friction.

Vernotte [6] has defined the coefficient p as proportional to the effusivity of each material in contact (Eq. (2))

$$p = \frac{1}{1 + \frac{\xi_p}{\xi_d}} \tag{2}$$

2.1.2 Imperfect Contact. The constriction thermal effects due to asperities and the accumulation of wear particules to form a thin layer (usually called third body) at the interface between the two primary bodies are in contradiction with the assumption of thermal continuity. Experimental results highlight a macroscopic thermal gradient between the two body surfaces [2] which is com-

Contributed by the Tribology Division for publication in the ASME JOURNAL OF TRIBOLOGY. Manuscript received by the Tribology Division May 27, 2003; revised manuscript received December 9, 2003. Associate Editor: M. R. Lovell.

Table 1 Parameters of automotive brake application [12]

Inner disc diameter: 132 mm	Initial speed: 100 $km \cdot h^{-1}$	Peak power time: 0.5 s
Outer disc diameter: 227 mm	Braking time: 3.96 s	Mean sliding radius: 94.5 mm
Disc thickness: 11 mm	Deceleration: 7 $m \cdot s^{-2}$	Sliding length: 37 mm
Pad thickness: 10 mm	Total energy: 165 kJ	Convection coefficient: 60 $W \cdot m^{-2} \cdot K^{-1}$

monly modelled by using a thermal contact resistance. This resistance is experimentally measured by evaluating temperature at disc and pad surfaces (respectively T_d and T_p) [7,8]. Thermal contact resistance, R_c, is expressed by (Eq. 3)

$$R_c = \frac{T_p - T_d}{\phi_i} \tag{3}$$

with ϕ_i the heat flux across the interface

Analytical determinations of R_c are given in the literature, under conditions of thermal steady state and for simplified geometries of asperities [8]. Unfortunately, braking problem is typically a thermal transient problem, which is held during a very short time compared to steady state conditions. The limitations of the thermal resistance concepts are essentially: the linear evolution of the thermal gradient between the two surfaces, the absence of thermal interface inertia consideration. Many experimental studies have pointed out these deficiencies of the pure thermal resistance scheme [9].

That is why, in the most studies dealing with braking analysis, analytical solutions have been developed using perfect contact, less realistic but of an easier development [10,11].

2.2 Automotive Brake Application. As an illustration, let us consider the automotive disc brake issued from literature data [12]. The details of the dimensions and operating conditions are given in Table 1.

The disc material is steel while the pad material is made of an organic matrix composite. Their physical properties at room temperature are detailed in Table 2.

2.3 Contact Temperature of a Disc Brake: Analytical Solution. The most successful models predicting surface temperatures in disc brakes are due to Newcomb [10] and Limpert [11]. In these models, only the macroscopic solids geometries and macroscopic boundary conditions are required. Assuming a perfect contact (i.e., constant heat flux partition between the two parts during braking), the friction mechanisms at the interface are simplified by considering separately the rotor (disc) and the stator (pads). The heat dissipated by each component is obtained via Eq. (2). As the contact surface of the two components (respectively S_d and S_p) are quite different, the pad density and conductivity are corrected by introducing the disc to pad surface ratio by means (Eq. (4))

$$\lambda_p' = \frac{\lambda_p}{S_d/S_p}; \quad \rho_p' = \frac{\rho_p}{S_d/S_p} \tag{4}$$

Table 2 Thermal physical properties

	Disc	Pad
Conductivity ($W \cdot m^{-1} \cdot K^{-1}$)	43.5	12
Density ($kg \cdot m^{-3}$)	445	900
Heat capacity ($J \cdot kg^{-1} \cdot K^{-1}$)	7850	2500

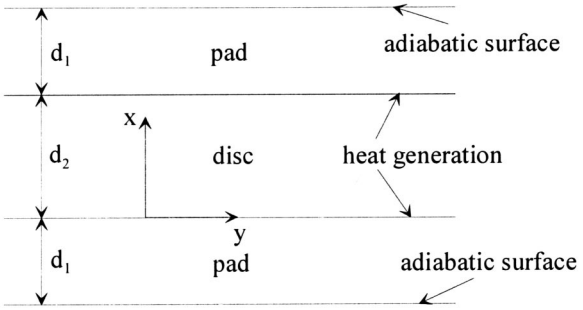

Fig. 1 Newcomb model scheme

The heat flux partition, p, becomes (Eq. (5))

$$p = \frac{\xi_d S_d}{\xi_p S_p + \xi_d S_d} \tag{5}$$

2.3.1 Newcomb Model. If each pad exerts a constant frictional force, the rate of heat generation q at the interface linearly decreases with time t: $q = q_0(1 - t/t_b)$. A first approximation in the determination of the temperatures on the disc is obtained by solving the problem of a linear one-dimensional heat flow through a composite solid made of three infinite layers with the two interfaces subjected to a thermal flux decreasing linearly with time. The two outer boundaries are considered as adiabatic surfaces (Fig. 1).

The resolution of the heat equation coupled to boundary conditions with assumption of equal temperature at contact interfaces gives the following relationship for the surface temperature (Eq. (6)):

$$\begin{aligned} T_s = \Bigg| & \frac{q_0 a_d^{1/2}}{\lambda_d(1+\sigma)} \Bigg\{ \frac{2t^{1/2}}{\pi^{1/2}} \left(1 - \frac{2}{3}\frac{t}{t_b}\right) + \frac{4t^{1/2}}{(1+\sigma)} \left[i \cdot \operatorname{erfc}(2\kappa_d) - \sigma \cdot i \operatorname{erfc}(2\kappa_p) - 4\frac{t}{t_b}\left(i^3 \operatorname{erfc}(2\kappa_d) - \sigma i^3 \operatorname{erfc}(2\kappa_p)\right) \right] \\ & + 2(1-2A^2)t^{1/2} \left[i \operatorname{erfc}(2(\kappa_p+\kappa_d)) - 4\frac{t}{t_b} i^3 \operatorname{erfc}(2(\kappa_p+\kappa_d)) \right] + 4Bt^{1/2} \left[i \operatorname{erfc}(4\kappa_d) - \sigma \cdot i \operatorname{erfc}(4\kappa_p) \right. \\ & \left. - 4\frac{t}{t_b}\left(i^3 \operatorname{erfc}(4\kappa_d) - \sigma \cdot i^3 \operatorname{erfc}(4\kappa_p)\right) \right] + 2(1+3A-A^2)t^{1/2} \left[i \operatorname{erfc}(2(2\kappa_d+\kappa_p)) - 4\frac{t}{t_b} i^3 \operatorname{erfc}(2(2\kappa_d+\kappa_p)) \right] \\ & + 2(1-3A-A^2)t^{1/2} \left[i \operatorname{erfc}(2(2\kappa_p+\kappa_d)) - 4\frac{t}{t_b} i^3 \operatorname{erfc}(2(2\kappa_p+\kappa_d)) \right] + 4Ct^{1/2} \left[i \operatorname{erfc}(6\kappa_d) - 4\frac{t}{t_b} i^3 \operatorname{erfc}(6\kappa_p) \right] + \ldots \Bigg\} \end{aligned} \tag{6}$$

where

$$\sigma=\frac{\lambda_p}{\lambda_d}\left(\frac{a_d}{a_p}\right)^{1/2},\quad \kappa_d=\frac{d_2}{4(a_d t)^{1/2}},\quad \kappa_p=\frac{d_1}{4(a_p t)^{1/2}},\quad A=\frac{1-\sigma}{1+\sigma},\quad B=\frac{1-\sigma}{(1+\sigma)^2},\quad C=\frac{(1-\sigma)^2}{(1+\sigma)^3}$$

$$\mathrm{i^n\,erfc}(x)=\int_x^\infty i^{n-1}\,\mathrm{erfc}(y)\cdot dy$$

$$i^0\,\mathrm{erfc}(x)=\mathrm{erfc}(x)=\frac{2}{\pi^{1/2}}\int_x^\infty \exp(-y^2)dy$$

2.3.2 LIMPERT Model. The problem solved by Limpert is illustrated in Fig. 2 for a brake disc. Both sides of the rotor are heated by the flux (q_0) and cooled by convection (h_r). Brake temperature evolutions can be computed at any location beneath the friction surface [11].

In this model, firstly assuming a constant heat flux, a temperature response, $\theta_0(z,t)$, is expressed by summing two functions (Eq. (7)).

$$\theta_0(z,t)=\psi(z,t)+\phi(z,+\infty) \tag{7}$$

The function $\phi(z,+\infty)$ represents the steady-state temperature of the disc. The function $\psi(z,t)$ represents the difference between the steady-state and transient temperature of the disc.

Getting $\theta_0(z,t)$ requires the following conditions:

- the temperature is only a function of the coordinate normal to the friction surface and time t
- the heat transfer coefficient h_r is constant
- the heat flux is in the direction normal to the friction surface
- the thermal properties of disc and pads are constant and evaluated at mean temperature
- the room temperature T_∞ is constant

The solution of such a problem is therefore (Eq. (8)).

$$\theta_0(z,t)=\frac{q_0}{2\cdot h}\left[2\left(\frac{2\,\theta_i h_r}{q_0}-1\right)\sum_{n=1}^{\infty}\left(\frac{\sin(k_nL)}{k_nL+\sin(k_nL)\cos(k_nL)}\times e^{-\xi_d\cdot k_n^2\cdot t}\cos(k_nz)+1\right)\right] \tag{8}$$

where $\theta_i=T_i-T_a$ is the initial thermal difference between brake and ambient air (°C)

The value of k_nL is determined from the transcendental equation (Eq. (9))

$$(\mathrm{k_nL})\tan(\mathrm{k_nL})-\mathrm{h_rL}/\lambda_\mathrm{d}=0 \tag{9}$$

By applying Duhamel's theorem in Eq. (8), the temperature response resulting from a linearly decreasing heat flux is (Eq. (10))

$$T(z,t)=2\,\theta_0(z,t)-\frac{q_0}{t_f h}\left[t-2\sum_{n=1}^{\infty}\frac{\sin(k_nL)}{k_nL+\sin(k_nL)\cos(k_nL)}\times\frac{1-e^{-\xi_d k_n^2 t}}{\xi_d k_n^2}\cos(k_nz)\right] \tag{10}$$

2.3.2 Comparison Between Newcomb and Limpert Models. According to Eq. (5), 93.4 percent of the total heat flux is assumed to be dissipated by the disc.

Figure 3 shows the surface temperature evolution with respect to time when using Newcomb and Limpert models (respectively Eq. (6) and Eq. (9)).

The good agreement between the two models is the consequence of the convective coefficient introduced in Limpert's model that does not affect the temperature evolution during a single stop.

3 F.E. Thermal Modeling of Disc Brakes

3.1 Main Assumptions. Generally, the standard finite element models used for disc brake thermal analysis only consider the disc and the pads. The high rotating speed of disc allows the angular thermal gradient to be neglected and the problem to be treated as an axial symmetrical cross-section model (Fig. 4).

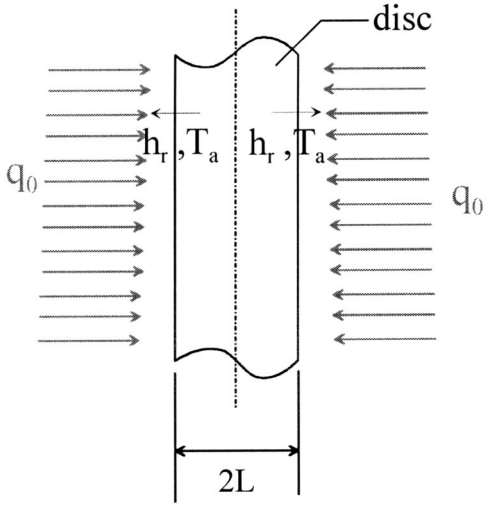

Fig. 2 Limpert model scheme

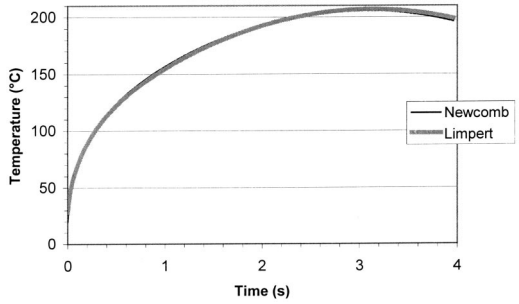

Fig. 3 Analytic surface temperature evolutions

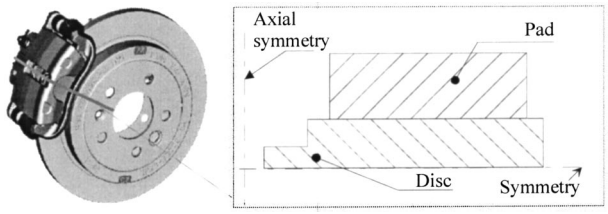

Fig. 4 Axial symmetrical model

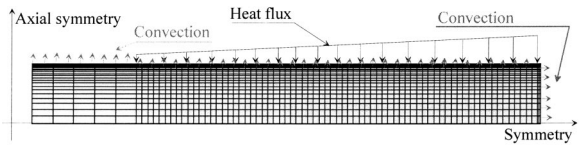

Fig. 5 Axial symmetrical F.E. model of disc

3.2 Model Description. In a first step, only the disc is modelled as described in Fig. 5. The influence of the pad is implicitly taking into account by the heat flux partition coefficient defined by Eq. (5).

The heat flux generated at any point on the friction surface depends on the local friction force and the sliding speed. As the goal of this study is to compare mean temperature evolutions of disc and pad surfaces, the pressure distribution between the pad and the disc is assumed to be uniform, and the friction coefficient is assumed to be constant.

The convection coefficient on the friction surface is estimated using the following empirical correlation [11] (Eq. (11)):

$$h_r = 0.015 \frac{\lambda_{\text{air}}}{2\pi r_m} \left(\frac{2\pi r_m^2}{\upsilon_{\text{air}}} \right)^{0.8} \tag{11}$$

3.3 Results and Comparison With Analytical Model. In order to take into account the engagement time parameter corresponding to the time of inlet pressure in the cylinder, two cases have been studied (by means with and without engagement time). Evolutions of mean contact temperatures at the disc surface issued from the F.E. analysis are shown in Fig. 6 and compared to the analytical results derived from Newcomb's model.

When considering no engagement time, a quite good agreement is observed between analytical and F.E. results. The slight highlighted divergence is the consequence of the thermal volumic diffusion, acting on inner and outer diameter of the disc in the F.E. model, while the heat flux is assumed to be uniform on the whole disc surface in the analytical one.

If an engagement time is introduced, the divergence is essentially more important at the beginning when the temperature rises more slowly.

3.4 Conclusion. Under very restrictive assumptions, analytical models lead to rather complex temperature formulations. In F.E. models, introduction of realistic boundary conditions is easier. However, in both cases, assumption of perfect contact is really a bolt which has to be raised.

Indeed, experimental thermal measurements on TGV disc brakes have shown a significant temperature gap between the disc and the pad surfaces [2] (Fig. 7). In these experiments, temperature on the disc surface have been measured using an infrared camera and those inside the pads, with thermocouples at 2.2 mm depth from the surface. As the pad temperature in this located zone is already higher than on the disc surface one may expect a more significant gap between the two surface temperatures.

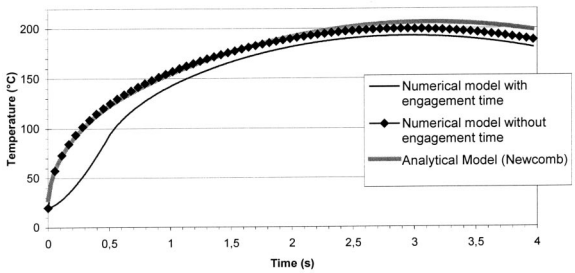

Fig. 6 Mean contact temperature evolution

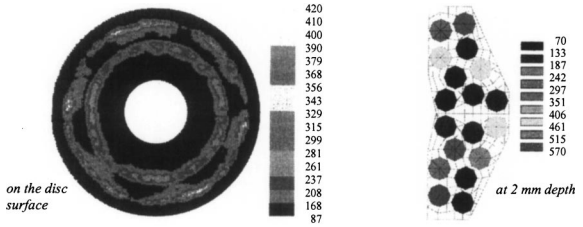

Fig. 7 Thermal measures on the disc surface and in the pad, at the time of maximal temperature (°C)

Such a thermal gradient between the two components surfaces may be explained by the existence of a third body [13] since analysis of disc surface after several brakings have shown local zones of wear particles (Fig. 8).

4 Model Including Third Body

4.1 The Third Body. The basic configuration of the mechanical approach of tribology stipulates that the two first bodies are not in contact but always separated by a third one constituted by detached particles [13].

The third body is a volume of material that separates the first bodies and transmits the load while accommodating the greater part of their speed difference. In a mechanical approach, it is sometimes of interest to geometrically distinguish the screens (oxides layers, etc.) whose thickness is usually less than $50 \cdot 10^{-6}$ mm and the solid particles circulating in the contact, which constitutes a "more and less continuous film" of about 0.01 mm thickness [15,17]. The flow mechanisms of the third body are well described in literature [13].

4.2 Thermal Aspects. Ryhming [14] analyzed the heat conduction problem of a tool work-piece interaction by assuming the presence of a thin boundary layer between the tool wear-flat and the workpiece. A constant volumic rate of heat generation is assumed in the layer which is constituted of a very fine powder. Its thermal properties may significantly differ from those of the tool and the work-piece.

Ryhming analytically studied a bidimensional problem where the shape of the tool is approximated as a narrow band moving over the work-piece surface. A thin boundary layer of thickness, *d*, is taken into account (Fig. 9).

A temperature gap between tool and work-piece surfaces was pointed out. The maximal temperature is reached in the interface and strongly depends on the layer material properties and thickness.

4.3 F.E. Model Including Third Body. The F.E. model is axial-symmetric as previously described in section 3.2. The third body, modelled as a volumic layer, is assumed to be homogeneous and uniformly distributed between the disc and the pad (Fig. 10).

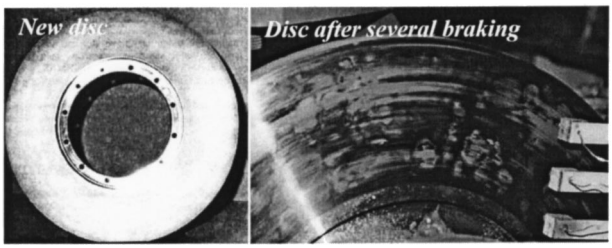

Fig. 8 Particles debris on the disc

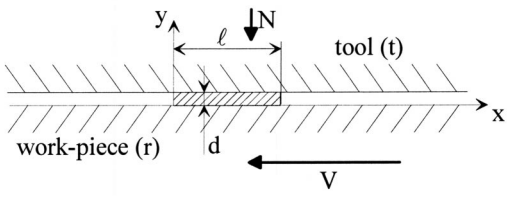

Fig. 9 Geometry considered by Ryhming

The thermophysical properties of the layer are introduced in the model using the following experimental values measured by Day [15]:

- Conductivity: 0.07 $W \cdot m^{-1} \cdot K^{-1}$
- Specific Heat: 1000 $J \cdot kg^{-1} \cdot K^{-1}$
- Density: 0.1 $kg \cdot m^{-3}$

A third body thickness of 0.01 mm has been used by Day [15]. This value is in agreement with that measured by Noll [17]. In the present model, the same third body thickness has been retained in a first step.

Such a set of values leads to an equivalent thermal conductance of about 7000 $W \cdot m^{-1} \cdot K^{-1}$ which is in agreement with the range of 1000 to 50,000 $W \cdot m^{-2} \cdot K^{-1}$ given by Holman [18].

Assuming an uniform pressure in the contact leads to consider that the total heat generated by friction is dissipated uniformly in the third body layer.

Temperature evolutions of the disc and the pad surfaces are described in Fig. 11. As the heat flux is meanly dissipated by the disc (94 percent), disc temperatures are almost the same as those obtained with assumption of perfect contact. However, pad temperature is higher due to the third body layer that acts as a thermal resistance (as the pad effusivity is weaker, its temperature quickly rises in the same form as the heat flux evolution). In agreement with both Day results [15], Ryhming consideration [14] and experimental investigations [16], the existence of a surface thermal gradient has been pointed out (with a maximal gradient value up to 400°C).

4.4 Third Body Thickness Sensitivity. The influence of the third body layer thickness has been investigated. High range of thickness values are considered in order to study thermal effects in a three bodies model. The resulting temperature evolutions are shown in Fig. 12(a) for the disc and Fig. 12(b) for the pad.

As the thickness parameter increases the disc surface temperature decreases. For the pad, two opposite effects are observed: up to 0.3 mm of layer thickness, the surface temperature increases while it decreases among this value. In the first range, the heat flux absorbed by the pad grows up (Fig. 13(a)), since the thermal barrier effect increases with thickness. The storage ability of the third body is quite weak (Fig. 13(b)).

Among 0.3 mm thickness, maximal pad temperature decreases even if thermal resistance effect is higher. This is due to the heat flux absorbed by the third body that becomes significant for high thickness as illustrated in Table 3. If we focus on the transient phenomenon, Fig. 13(b) shows that heat flux in the third body

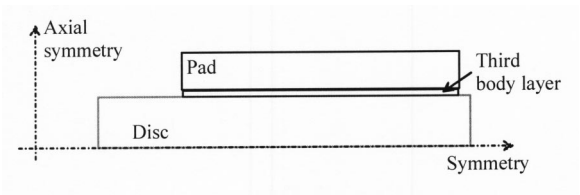

Fig. 10 Model with third body layer

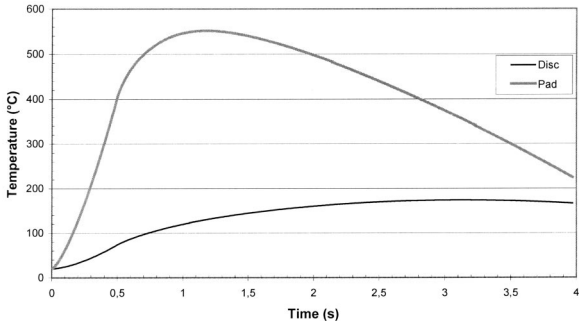

Fig. 11 Disc and pad surface temperature evolutions

increases at the beginning of braking and consequently decreases into the pad (Fig. 13(a)) and into the disc. During the second half-braking, the heat flux absorbed by the third body is dissipated into the disc and the pad. The heat flux ratio into the pad grows up with third body thickness as shown in Fig. 13(a) but as braking power linearly decreases with time, maximal temperature is weaker.

In the same way, as thickness increases, time to reach the maximal temperature in the pad first decreases before increasing (Fig. 12(b)).

Maximal temperature are very high beyond a thickness of 0.05 mm. Such values are not realistic according to the material degradations but it highlights the main trends about the third body influence, and particularly the energy storage phenomena in the third body and the competition with regard to thermal resistance effect.

Figure 14 shows the temperature distribution in the third body for two thicknesses of 0.01 and 0.1 mm. In both cases, maximal temperature is obtained inside the third body. It agrees with Ryhming results [14] but not with Day one [15], illustrating the difference between a volumic model and an equivalent thermal resistance approach.

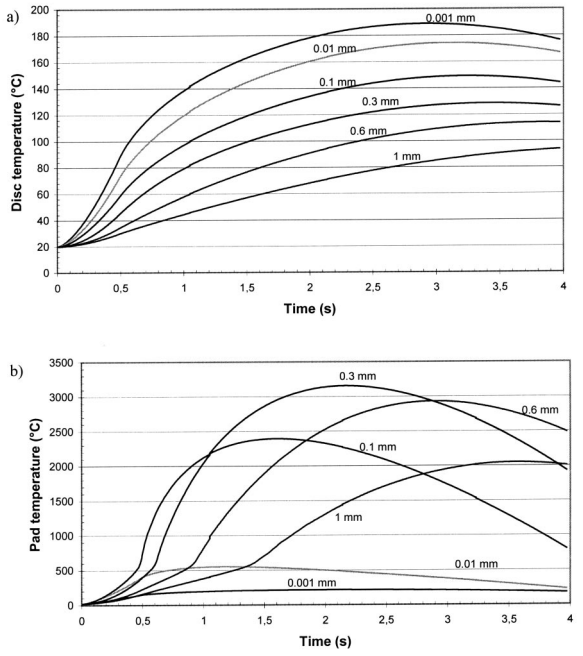

Fig. 12 Disc and pad temperature evolution for varying third body thickness

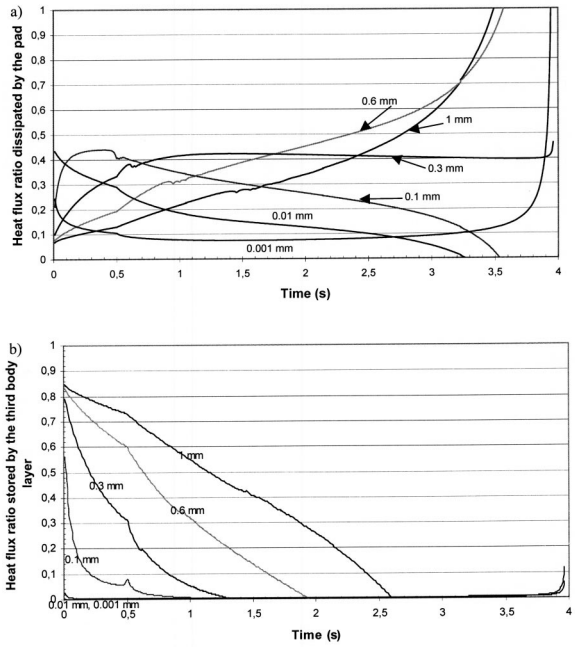

Fig. 13 Heat flux ratio dissipated by the pad and stored by the third body layer

For thin layers, maximal temperature is obtained near the pad surface because of its weaker effusivity. As thickness increases, maximal temperature moves to the middle of third body layer.

4.5 Third Body Conductivity Sensitivity. The sensitivity of the third body conductivity has been investigated in the range of 0.01 to 7 $W \cdot m^{-1} \cdot K^{-1}$. While the influence is low on the disc temperature (Fig. 15(a)) this parameter is quite influent as shown in Fig. 15(b) because of the thermal barrier effect.

5 Conclusion

The aim of this work was to deal with the thermal modelling of two components in sliding contact. In such a problem, two main classical approaches are commonly used (1) perfect contact leading to equal surface temperature of the components, and (2) thermal resistance introducing a temperature gap between the two surfaces.

The model described here, has introduced the third body acting between the primary bodies as a continuous thin layer. Thermal model is volumic with uniform heat generation inside the third body layer. Contrary to the classical models, it allows to get a temperature evolution along the third body thickness and to point out the notion of energy storage inside this body.

The results are mainly sensitive to two parameters: the third body layer thickness and its conductivity.

When taking parameters values found in literature (0.01 mm thickness and conductivity of 0.07 $W \cdot m^{-1} \cdot K^{-1}$), results exhibit

Table 3 Energy ratio stored in the third body layer during braking time

Third body thickness (mm)	Heat flux absorbed by the third body (%)
0.001; 0.01	0.4
0.1	0.6
0.3	3.0
0.6	12.5
1	32.8

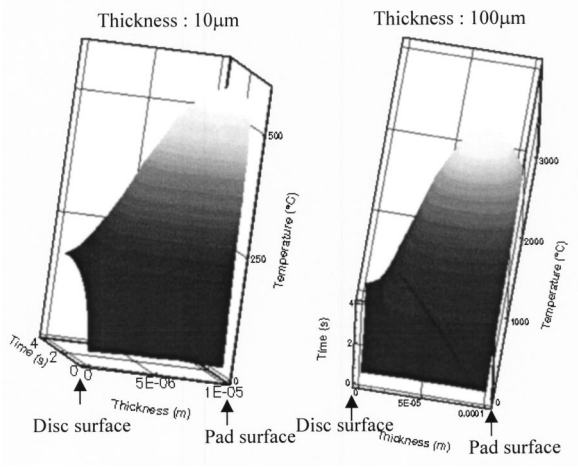

Fig. 14 Temperature distribution in the third body

thermal gradients between the two primary body surfaces in agreement with experimental observations found in literature and obtained by the authors.

Thickness parameter significantly acts on temperature levels. For realistic weak thickness, maximum temperature is obtained inside the third body, near the pad surface due to its weaker effusivity.

Results have shown that introducing a third body model leads to high levels of temperature that probably give material degradations. If we consider that contact is not uniform with very low friction surfaces compared to the apparent ones, temperatures would be much higher. It illustrates the necessity to enrich the models by taking into account material degradations and real contact surfaces evaluations.

Heat generation has been given uniform in the third body. Another way would be to use velocity accommodation between the two primary bodies. The continuity of the third body model has still to be discussed if we consider its heterogeneity with powders

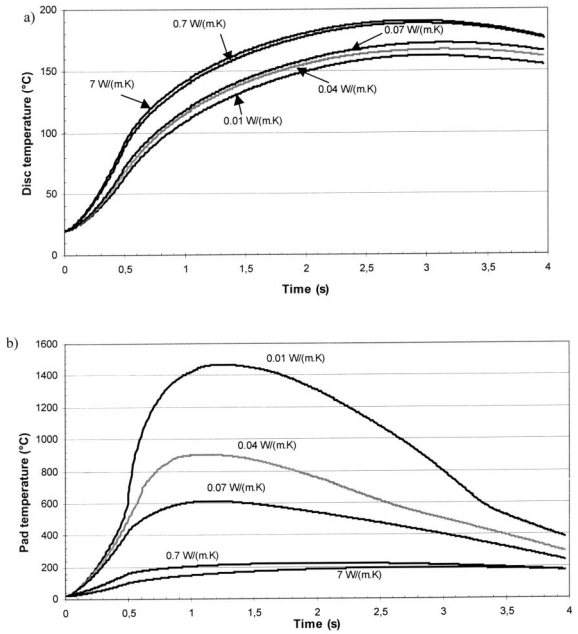

Fig. 15 Disc and pad temperature evolution for various third body conductivities

and slabs. Nevertheless, the first results seems promising since they are in agreement with macroscopic thermal observations.

Acknowledgment

Special thanks to Y. Berthier from INSA LYON LMC UMR CNRS 5514 for helpful discussions.

Nomenclature

a = thermal diffusivity ($m^2 \cdot s^{-1}$)
c = specific heat ($J \cdot kg^{-1} \cdot K^{-1}$)
d = thickness (m)
E_c = kinetic energy (J)
erf(●) = error function
m = mass of the vehicle associated with each brake disc (kg)
p = heat flux partition coefficient (dimensionless)
Q = heat (J)
q = heat flux density dissipated by disc ($W \cdot m^{-2}$)
q_0 = heat flux density dissipated by disc at time t=0 ($W \cdot m^{-2}$)
R_c = thermal contact resistance ($K \cdot W^{-1}$)
r_m = mean radius (m)
S = contact surface (m^2)
T = temperature (°C)
t = time (s)
t_b = braking time (s)
V_0 = vehicle initial speed ($m \cdot s^{-1}$)

Greek Symbols

λ = thermal conductivity ($W \cdot m^{-1} \cdot K^{-1}$)
ϕ = heat flux (W)
ξ = disc thermal effusivity ($J \cdot m^2 \cdot K^{-1} \cdot s^{-0.5}$)
ρ = disc volumic density ($kg \cdot m^{-3}$)

Subscripts

d = disc
p = pad

References

[1] Kennedy, F. E., 1984, ''Thermal and Thermomechanical Effects in Dry Sliding,'' Wear, **100**, pp. 453–476.
[2] Dufrénoy, P., and Weichert, D., 1995, ''Prediction of Railway Disc Brake Temperatures Taking the Bearing Surface Variations Into Account,'' IMechE, Part F: Journal of Rail and Rapid Transit, **209**, pp. 67–76.
[3] Berthier, Y., 2001, *Background on Friction and Wear*, Lemaitre Handbook of Materials Behavior Models, Lemaitre Academic Press, pp. 676–699, Chpt. 8.
[4] Descartes, S., and Berthier, Y., 2001, ''Frottement et usure étudiés à partir de la rhéologie et des débits de 3ème corps solide,'' Matériaux & Techniques, SIRPE ed., Paris, **1-2**, pp. 3–14.
[5] Archard, J. F., 1958, ''The Temperatures of Rubbing Surfaces,'' Wear, **2**, pp. 438–455.
[6] Vernotte, P., 1956, *Calcul numérique, calcul physique: Application à la thermocinétique*, Publications scientiques et techniques du ministère de l'air.
[7] Bardon, J. P., 1994, ''Bases physiques des conditions de contact thermique imparfait entre milieux en glissement relatif,'' Rev. Gén. Therm. Fr., **386**, pp. 85–91.
[8] Laraqi, N., 1996, ''Phénomène de constriction thermique dans les contacts glissants,'' Int. J. Heat Mass Transfer, **39**(17), pp. 3717–3724.
[9] Cames-Pintaux, A. M., and Padet, J. P., 1980, ''Etude des contacts thermiques en régime transitoire. Proposition d'un modèle thermiquement équivalent,'' Int. J. Heat Mass Transfer, **23**, pp. 981–990.
[10] Newcomb, T. P., 1959, ''Transient Temperatures Attained in Disk Brakes,'' Br. J. Appl. Phys., **10**, pp. 339–340.
[11] Limpert, R., 1992, *Brake Design and Safety*, Elsevier Editions, New York.
[12] Tirovic, M., and Day, A. J., 1990, ''The Calculation of Temperatures in Brakes,'' Second One-Day Workshop on Disc and Drum Brake Performance, University of Bradford, UK.
[13] Berthier, Y., 1988, ''Mécanismes et tribologie,'' Ph.D. thesis, N° 88ISAL0050, INSA de Lyon France.
[14] Ryhming, I. L., 1979, ''On Temperature and Heat Source Distributions in Sliding Contact Problems,'' Acta Mech., **32**, pp. 261–274.
[15] Day, A. J., 1983, ''Energy Transformation at the Friction Interface of a Brake,'' Ph.D. thesis, The Loughborough University of Technology.
[16] Majcherczak, D., Dufrénoy, P., and Naït-Abdelaziz, M., ''Thermal Simulation of a Dry Sliding Contact Using a Multiscale Model—Application to the Braking Problem,'' *Thermal Stresses 2001*, Osaka Prefecture University, Japan pp. 437–440.
[17] Noll, N., 1997, ''Conception et naissance d'un contact tribologique—Rôle des écrans de surface,'' Ph.D. thesis, INSA de LYON, France.
[18] Holman, J. P., *Heat Transfer*, 8th ed., MacGraw-Hill.